

Research article**Improvement of the Electrical Properties of ZnO Nanomaterials with Fe by Co-precipitation Method**Pitchaporn Kingpho¹ and Buppachat Toboonsung^{1,2*}¹Program of Science Education, Graduate School, Nakhon Ratchasima Rajabhat University, Nakhon Ratchasima, Thailand²Program of Physics, Faculty of Science and Technology, Nakhon Ratchasima Rajabhat University, Nakhon Ratchasima, Thailand

Received: 26 May 2024, Revised: 11 August 2024, Accepted: 1 November 2024, Published: 9 December 2024

Abstract

Fe-doped ZnO nanomaterials were prepared by the co-precipitation method. The experiments used a solution of 0.5 M for ZnCl₂, doped with FeSO₄ in proportions of 0-100 wt.%, followed by the addition of 1 M for NaOH solution until a pH of 12 was reached. Next, the precipitated substances were calcinated at 550°C for 3 h in air. SEM image analysis showed that the nanoparticles formed in the condition of pure ZnO and Fe₂O₃ whereas rod-shaped formed with Fe doping. Nanoparticles of ZnO transformed into nanorods when doped with Fe. EDS analysis detected Fe under the conditions of 3 and 5 wt.% doping. XRD patterns of ZnO and all doping of Fe in ZnO nanostructures were corresponded to a hexagonal wurtzite structure of ZnO which showed crystallite size in the range of 25-29 nm. The electrical properties of Fe-doped ZnO nanostructures were identified by the spectroscopy measurements of fluorescence and ultraviolet-visible absorption, and the electrical conductivity was calculated. It was found that Fe doping at 3 wt.% produced the lowest energy band gap (based on spectroscopy results) and this condition was associated with the highest electrical conductivity of $0.21 \times 10^{-3} (\Omega \cdot \text{cm})^{-1}$ which was calculated from the measurement of electrical resistance by two probes. Therefore, Fe doping can improve the electrical properties of ZnO nanostructures.

Keywords: co-precipitation; Fe-doped ZnO; electrical conductivity; energy band gap; fluorescence spectroscopy

1. Introduction

Currently, electronic devices are increasingly being developed from nanomaterials that improve electrical properties such as gas sensors (Nakate et al., 2021), supercapacitors (Khan et al., 2022a), solar cells (Mahajan et al., 2022), optoelectronic devices (Khan et al., 2022b) and anti-bacterial films (Alavi et al., 2019, Nadeem et al., 2021). Titanium dioxide (TiO₂), nickel oxide (NiO), copper oxide (CuO) and zinc oxide (ZnO) nanomaterials were favorites due to their wide band gap (Toboonsung & Singjai, 2011; Meybodi et al., 2012; Sugumaran et al., 2021), excellent optical, electrical and magnetic properties

*Corresponding author: E-mail: buppachat.t@nrru.ac.th
<https://doi.org/10.55003/cast.2024.263485>

Copyright © 2024 by King Mongkut's Institute of Technology Ladkrabang, Thailand. This is an open access article under the CC BY-NC-ND license (<http://creativecommons.org/licenses/by-nc-nd/4.0/>).

(Toboosung, 2017; Divya et al., 2020; Pramothkumar et al., 2021). Moreover, research interest has been focused on improving the properties of ZnO by doping with other substances such as Cu (Sajjad et al., 2018), Fe (Saadi et al., 2020), Ni (Samanta et al., 2018), Co (Gaur et al., 2021) and Al (Mayandi et al., 2021) in order to modify its energy band (Sugumaran et al., 2021), its magnetic (Toboosung, 2017; Divya et al., 2020; Pramothkumar et al., 2021), electrical (Divya et al., 2020; Pramothkumar et al., 2021) and optical properties (Divya et al., 2020; Pramothkumar et al., 2021). Samanta et al. (2018) studied the magnetic and electric properties of Ni-doped ZnO nanoparticles. It was found that the dielectric constant decreased with increase in the doping concentration of nickel. The Ni doped ZnO nanoparticles indicated weak ferromagnetism. Saadi et al. (2020) synthesized Fe-doped ZnO nanopowders (ZnO:Fe), varying the doping concentrations from 0% to 10% and found improvement in the electrical conductivity with Fe doping. Gaur et al. (2021) were interested in Co-doped ZnO nanostructures which were synthesized by a simple chemical co-precipitation method. It was observed that the morphology of the nanoparticles was transformed from spherically shaped to rod-like shaped after Co doping. Nadeem et al. (2021) studied enhancements in the photocatalytic and antimicrobial properties and energy bandgap of Fe and Co co-doped ZnO nanoparticles. It was found that the energy bandgap (E_g) decreased with increasing Fe contents whereas it increased with Co concentration. Therefore, iron (Fe) as a doping agent became of interest as it could have the ability to modify the structure, morphology, optical properties, and electrical conductivity of ZnO (Sajjad et al., 2018; Divya et al., 2020; Saadi et al., 2020; Pramothkumar et al., 2021). In the past, various methods were introduced for the synthesis of undoped and doped ZnO nanostructures, including the co-precipitation (Sajjad et al., 2018; Saadi et al., 2020; Gaur et al., 2021; Mayandi et al., 2021; Nadeem et al., 2021), sol gel (Sangchay & Ubolchollakhat, 2016) and hydrothermal (Wang et al., 2013) methods. The co-precipitation method is a widely used synthesis technique because it is an easy method which can react with various substances at low temperatures. Therefore, it is suitable for doping Fe into ZnO nanostructures.

In this study, Fe doped ZnO nanomaterials were prepared by the co-precipitation method. Characterization techniques were used to study the morphology, chemical composition, crystal structure, optical properties, energy band gap values, and the electrical conductivities of the synthesized materials. Included were scanning electron microscopy (SEM), energy-dispersive X-ray spectroscopy (EDS), X-ray diffraction analysis (XRD), spectrofluorometry, ultraviolet-visible spectrophotometry and electrical resistivity measurement. The findings of this study could contribute to the understanding of the enhancement of the optical and electrical properties of Fe-doped ZnO nanomaterials. Furthermore, this knowledge might be useful in the future development of ZnO-based devices.

2. Materials and Methods

The co-precipitation method was used to synthesize Fe-doped ZnO nanostructures. The experiments used zinc chloride ($ZnCl_2$) 0.5 M solution as the initial substance (Saadi et al., 2020), and 0, 1, 3, 5 and 100 wt.% solutions of ferrous sulfate heptahydrate ($FeSO_4 \cdot 7H_2O$) were added as the dopant (Toboosung, 2017; Sajjad et al., 2018). The precipitation process was begun by mixing the solutions for 15 min with a magnetic stirrer (about 450 rpm), followed by the dropwise addition of 1 M sodium hydroxide (NaOH) until the pH reached 12 (Saadi et al., 2020; Pramothkumar et al., 2021). The mixture was then continuously stirred at room temperature for 30 min and left to precipitate. The precipitate

was washed several times with deionized water until a neutral pH was obtained, and was then calcined at 550°C for 3 h in an air atmosphere.

The morphology of the synthesized nanostructures was observed using scanning electron microscopy (SEM, JEOL JSM-7800F), and the chemical composition was determined by energy-dispersive X-ray spectroscopy (EDS, Oxford instrument). The crystal structure was analyzed using X-ray diffraction (XRD, Rigaku Smartlab) with Cu-K α radiation at 40 kV and 40 mA. The electrical properties were characterized by the energy band gap and the electrical conductivity. The energy band gap (E_g) was calculated from fluorescence spectrophotometry (JASGO FP8300) data and UV-Vis spectrophotometry (GENESYS 10S) data, which were used to explain the optical energies of emission and absorption, respectively. Additionally, the electrical conductivity was measured using 50 mg of sample powder, plastic insulation of area (A) 1x1 cm² and of thickness (d) 100 μ m, and copper plates as electrodes pressed with a hydraulic machine with a force of 2 kN. The direct electrical resistance was measured using an ohmmeter (UNI-T-UT70B, range of 0-40 Mega-Ohm, and open circuit voltage of approximately 3 volts) (Montes et al., 2011; Wang et al., 2013; Montes et al., 2016), as illustrated in Figure 1.

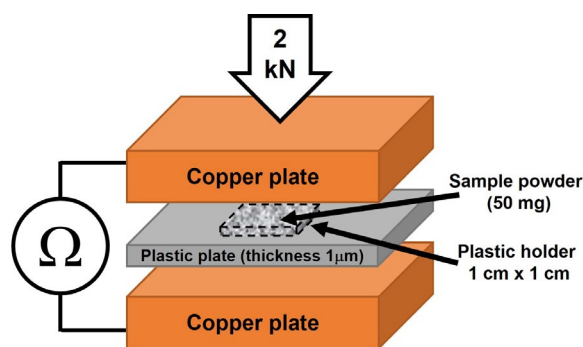


Figure 1. Schematic diagram of the direct electrical resistance measurement apparatus

3. Results and Discussion

3.1 SEM characterization

Figure 2 shows SEM images of nanostructures prepared using the co-precipitation method under different conditions of the purity of ZnO with Fe doping at 1-5 wt.%, comparing with Fe₂O₃ standard. It was found that the morphologies of the pure ZnO and pure Fe₂O₃ samples were observed to be nanoparticles (NPs) with diameters in the range of 10-150 nm and 20-40 nm, respectively (Figure 2(a) and Figure 2(e)). Doping ZnO with Fe concentrations ranging from 1 to 5 wt.% resulted in the formation of hexagonal nanorods (NRs) with diameters ranging from 170-330 nm and lengths ranging from 1-1.4 μ m, as shown in Figure 2(b-d). It was observed that the doping of Fe in ZnO resulted in a transition in morphology from nanoparticles (NPs) to nanorods (NRs), whereas in the non-doped samples, only nanoparticles were formed. The diameter and length of NRs increased with increase in the dosage of Fe. The SEM image clearly depicts NPs of Fe located on the surfaces of hexagonal NRs, and this phenomenon intensified with an increase in the volume of Fe, as shown in Figure 2(b-d). Many researchers have explained that the shape

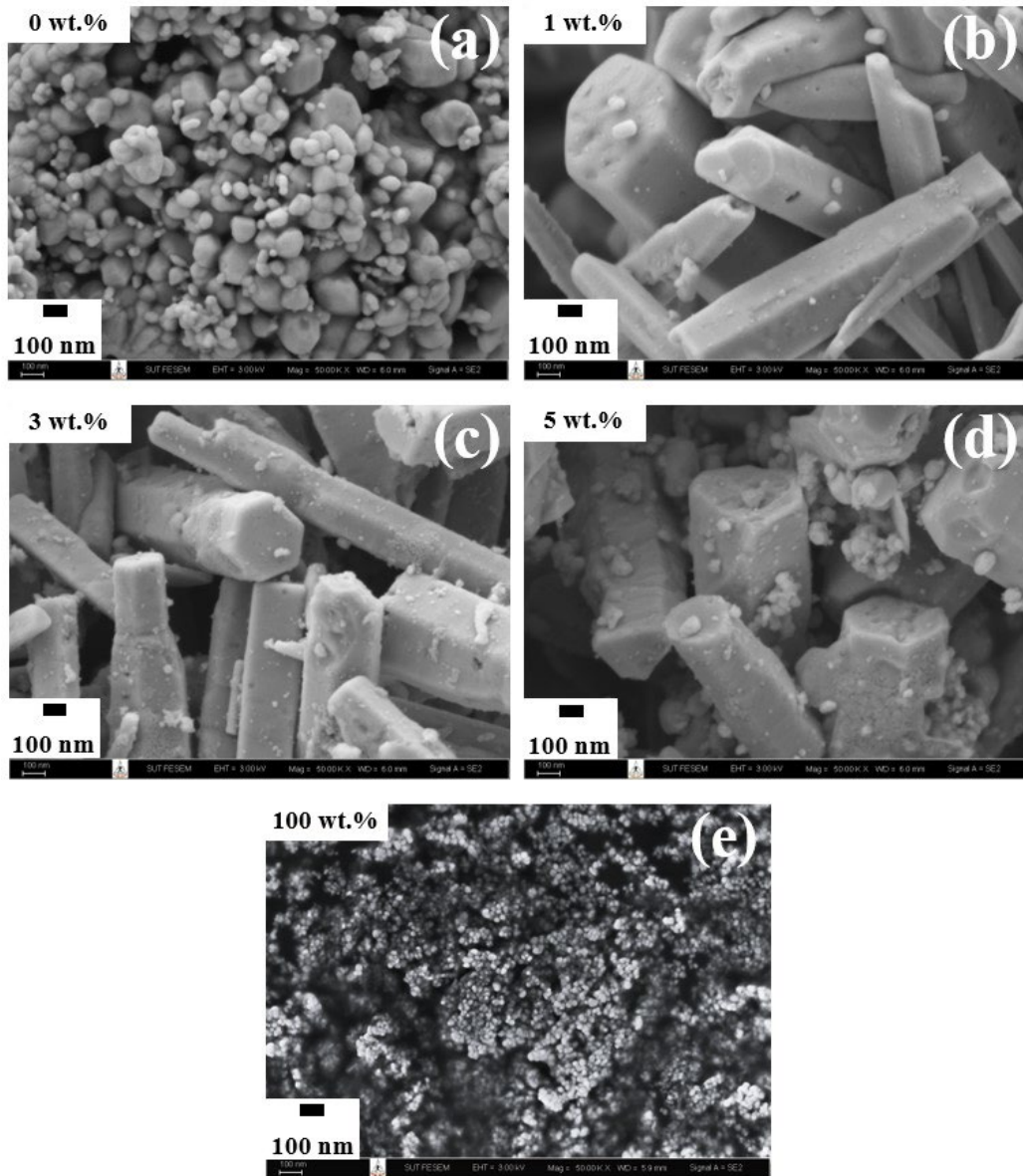


Figure 2. SEM images of the Fe-doped ZnO nanostructures of (a) 0 wt.% (ZnO), (b-d) 1-5 wt.% and (e) 100 wt.% (Fe₂O₃) at a magnification of 50,000X

of zinc oxide changes when it is mixed with other substances, which is a phenomenon explained by the theory of Ostwald Ripening (Kumar et al., 2013; Seid & Dejene, 2019; Ahmad & Maqsood, 2022). Ahmad & Maqsood (2022) reported similar morphological transformations in ZnO due to doping with elements like Ni using the co-precipitation method. These findings underscore the influence of dopants on the morphology of ZnO nanostructures which support the notion that the doping of materials can control the morphology of nanomaterials.

3.2 EDS analysis

Figure 3 illustrates the atomic percentages from energy-dispersive x-ray spectroscopy (EDS) graph, accompanied by an inset table detailing the elemental quantities in atomic percentage (at.%) and weight percentage (wt.%) for the Fe doped ZnO nanostructures corresponding to Figure 2(a-e). The EDS analysis, as presented in Figure 4, allows for a comparison of the elemental composition of samples based on atomic percentage. In Figure 3(a), zinc (Zn) peaks were evident at energy levels of 1.01 and 8.63 keV, while an oxygen (O) peak manifested at 0.52 keV. The atomic percentages of Zn and O, derived from EDS, were determined to be 45.40% and 54.60%, respectively, as indicated in the inset table of Figure 3(a) and Figure 4. This analysis clearly demonstrated that the ratio of the Zn and O elements by the atomic percentages (at.%) were as expected for ZnO composition. The EDS spectrum for iron (Fe), illustrated in Figure 3(e), displayed energy peaks at 0.71, 6.39, and 7.10 keV, with an oxygen peak occurring at the same energy level as observed in Figure 3(a). The atomic percentages of elemental Fe and O are presented in the inset table of Figure 3(e) and Figure 4, which indicated iron oxide in the form of Fe_2O_3 . Subsequently, Figure 3(b-d) depicted the EDS spectra for Fe-doped samples at 1-5 wt.%. It was noted that Fe was detected at the doping of 3 wt.% and 5 wt.%, but not in the 1 wt.% doped sample, as shown in Figure 4. The atomic percentage of elemental Fe was prominent in the 3 wt.% doping level, as delineated in Figure 4. This observation signifies the successful incorporation of the Fe at the 3 wt.% doping concentration, corroborating the efficacy of the doping process.

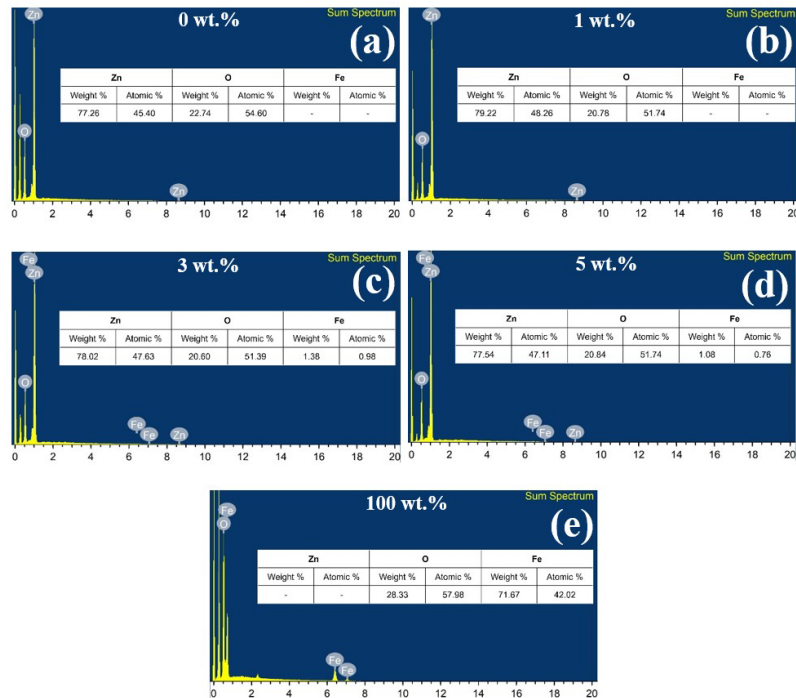


Figure 3. The EDS spectrum, along with the inset table showing the amount of each element in the sample in terms of weight percentage and atomic percentage, corresponding to each Fe-doped ZnO nanostructure shown in Figure 2.

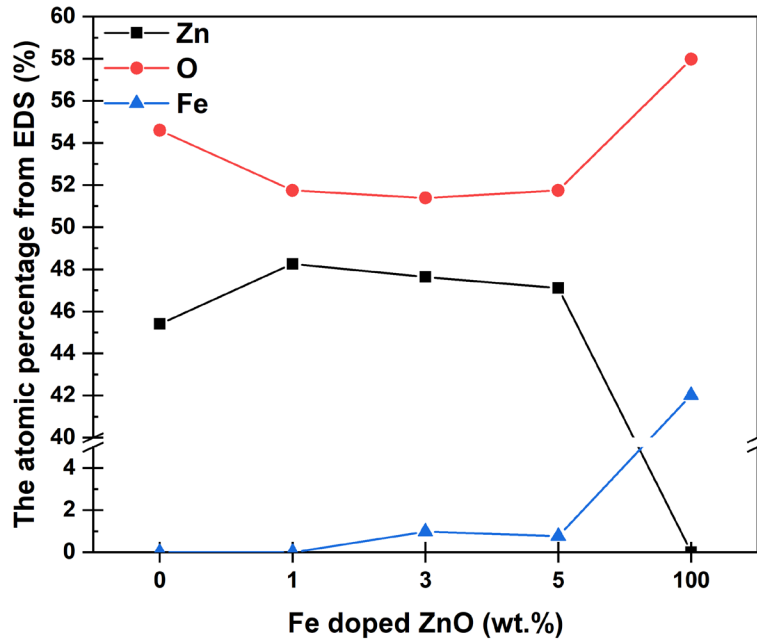


Figure 4. The atomic percentage of elements from EDS analysis of Fe-doped ZnO nanostructures, corresponding with Figure 3.

3.3 XRD measurement

Figure 5 shows XRD patterns for the 0, 1, 3, 5 and 100 wt.% Fe-doped samples, which corresponded to the SEM image and EDS spectra. The XRD patterns of the samples were recorded at room temperature in the 2θ ranges from 20° – 70° using Cu radiation with a wavelength of 1.54 \AA . It was found that the diffraction peaks of 0 wt.% Fe were shown in the planes (100), (002), (101), (102), (110), (103), (200), (112), and (201), which corresponded to the standard JCPDS data file No. 36–1451 for the hexagonal wurtzite crystalline structure of pure ZnO (Seid & Dejene, 2019; Ahmad & Maqsood, 2022). The X-ray diffraction pattern of 100 wt.% Fe showed the rhombohedral crystal structure of α - Fe_2O_3 and corresponded to the spectrum of JCPDS standard file No. 24-0072 with planes of (012), (104), (110), (113), (024), (116), (122), (214) and (300) (Mohammadi et al., 2023). The crystalline size of all samples was calculated by using the Scherrer equation:

$$D = K\lambda / \beta \cos\theta \quad (1)$$

where D is the crystalline size (nm), K is a constant taken to be 0.94, λ is the wavelength of x-rays (1.54 \AA), β is full width at half maximum intensity, θ is the Bragg's angle (Gaur et al., 2021). It was found that the crystalline sizes of pure ZnO and Fe_2O_3 samples were about 29 nm and 15 nm, respectively. The Fe-doped ZnO NRs at 1, 3 and 5 wt.% were of crystalline sizes of 25, 28 and 29 nm, respectively. It was noted that the crystalline sizes of the Fe-doped samples were similar to that of pure ZnO. Therefore, Fe-doped ZnO affected morphology but did not affect crystalline size.

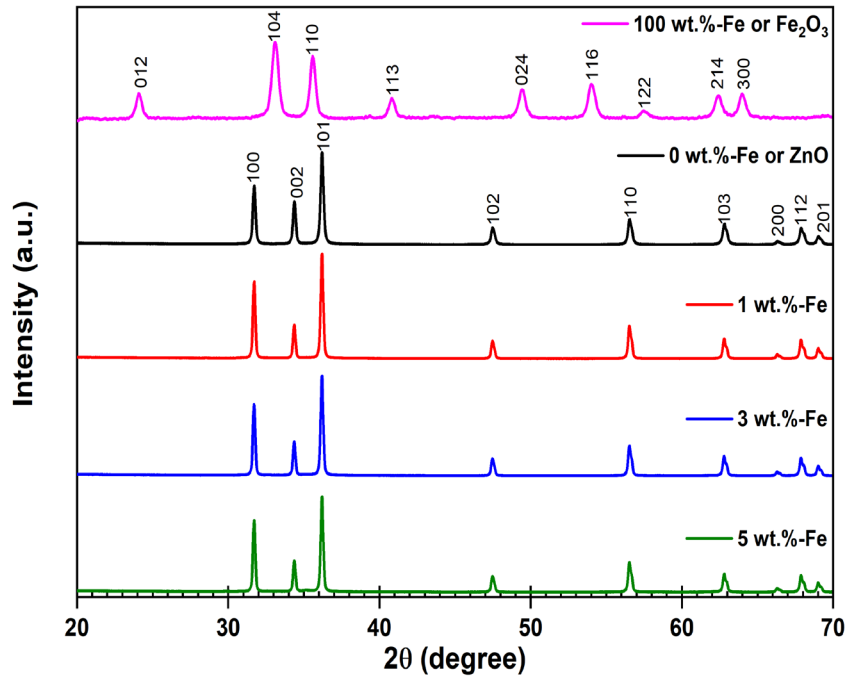


Figure 5. XRD patterns of Fe-doped ZnO at 0, 1, 3, 5 and 100 wt.%

3.4 Fluorescence spectrophotometer

Fluorescence spectrophotometer was employed to measure the luminescence and thus explain the energy band gap of the Fe-doped ZnO at 0, 1, 3, 5 and 100 wt.% doping, and the results are illustrated in Figure 6 (Kumar et al., 2013). The luminescence spectra of Fe-doped ZnO at 1, 3, and 5 wt.% resembled that the spectrum of the 0 wt.% sample, but they exhibited higher intensity. It was found that the doping of Fe increased with increasing of intensity and the highest luminescence intensity was observed for the 3 wt.% Fe-doped sample. The increase in luminescence intensity may be attributed to a reduction in oxygen vacancies and the presence of interstitial oxygen ions. Due to fewer oxygen vacancies, non-radiative recombination is reduced, leading to higher luminescence, while interstitial oxygen ions can further enhance this effect by facilitating radiative recombination (Baek et al., 2007; Cheng & Ma, 2009; Sharma & Jha, 2017). Consequently, the fluorescence spectrum was simulated using the three peaks of the Lorentz function, as shown in Figure 6(a-e) (Zeng et al., 2010; Gandhi et al., 2014; Niranjana et al., 2017; Alsmadi et al., 2020; Gaur et al., 2021; Singh & Singh, 2021). The three wavelengths (λ , unit as nm) were used to calculate the energy band gap (E_g , unit as eV) by using Planck's equation as follows (Zhu et al., 2009).

$$E_g = 1240 / \lambda \quad (2)$$

The energy band gap (E_g) values of the Fe-doped ZnO samples (0, 1, 3, 5, and 100 wt.%) are shown in Figure 6(f). The first peak (red line) showed the excitation energy, which was associated with electrons moving from the ground state to a higher energy level.

The excitation wavelength of Fe-doped ZnO of 0-5 wt.% samples was found in the range of 396-400 nm, corresponding to the ultraviolet (UV) region which represented a near band edge (NBE) transition and resulted in the radiative recombination of excitons (Zeng et al., 2010; Gandhi et al., 2014; Niranjana et al., 2017; Alsmadi et al., 2020; Gaur et al., 2021; Singh & Singh, 2021). However, the Fe₂O₃ sample (doped with 100 wt.% Fe) exhibited an excitation wavelength at 309 nm, as shown in Figure 6(e). For the NBE zone, it was observed that the samples with ZnO showed similar Eg values whereas pure Fe₂O₃ showed the highest Eg value, as shown in Figure 6(f).

Next, visible emission energy was explained by two peaks: the blue emission band (blue line) and green emission band (green line), which were associated with the liberation of fluorescent and phosphorescent energy, respectively. A number of reports stated that visible emission of ZnO was due to various intrinsic defects, such as oxygen vacancies (V_O), zinc vacancies (V_{Zn}), oxygen interstitials (O_i), zinc interstitials (Zn_i), and substitution of oxygen at the zinc position (O_{Zn}) (Wang et al., 2013; Seid & Dejene, 2019; Gaur et al., 2021). In this report, the blue emission band was caused by electronic transitions between defect levels in the band gap and was in the range of 442-449 nm for all samples, as shown in Figure 5(a-e). The blue emission band result from the creation of defect levels in ZnO, such as shallow donor levels between the valence and conduction bands, arising from Zn defects at the position of Zn interstitials (Zeng et al., 2010; Gandhi et al., 2014; Niranjana et al., 2017; Seid & Dejene, 2019; Alsmadi et al., 2020; Singh & Singh, 2021). It was found that increasing the Fe content caused the Eg values to increase from 2.76-2.80 eV which affected the oxygen vacancy, as shown in Figure 6(f).

The green emission resulted from a loss of energy during the return to the ground state (Gaur et al., 2021). All samples showed green emission in the range of 527-567 nm, as depicted in Figure 6(a-e). The appearance of green emission was attributed to transitions from shallow donors (Zn_i or Zn_i-related complex defects) to trapped holes in deep acceptor levels resulting from improved oxygen vacancy (V_O) development after doping (Zeng et al., 2010; Wang et al., 2013; Gandhi et al., 2014; Niranjana et al., 2017; Seid & Dejene, 2019; Alsmadi et al., 2020; Gaur et al., 2021; Singh & Singh, 2021). Interestingly, the doping of Fe in ZnO at 3 wt.% was shown to have the lowest Eg value in the green emission line, as shown in Figure 6(f). This could be attributed to a reduction in oxygen during the reaction mixture. Consequently, the oxygen vacancy defects were shown to enhance electronic properties (Asok et al., 2012; Thandavan et al., 2014).

3.5 Ultraviolet-visible spectrophotometer

Figure 7(a) presents the absorbance spectra obtained from the ultraviolet-visible (UV-VIS) spectrophotometry for Fe-doped ZnO samples at doping levels of 0, 1, 3, 5 and 100 wt.%. The pure Fe₂O₃ (100 wt.% Fe) NPs exhibited an absorption peak at the wavelengths of 386 nm. The Fe-doped ZnO NRs at 0, 1, 3 and 5 wt.% demonstrated absorption wavelengths at 396, 407 nm, 415 nm, and 377 nm, respectively. It was found that the redshift effect occurred due to the increasing concentration of Fe. The redshift phenomenon occurred by structural disorder in the ZnO lattice that generated electronic defect states in the forbidden region near the conduction and valence band, which affected the narrowing of band gap. Therefore, the energy band gap of ZnO was improved by the Fe doping (Singh & Singh, 2021). Notably, it was observed that the doping of Fe up to 3 wt.% resulted in the highest wavelength and absorption intensity, which then decreased at 5 wt.% of Fe.

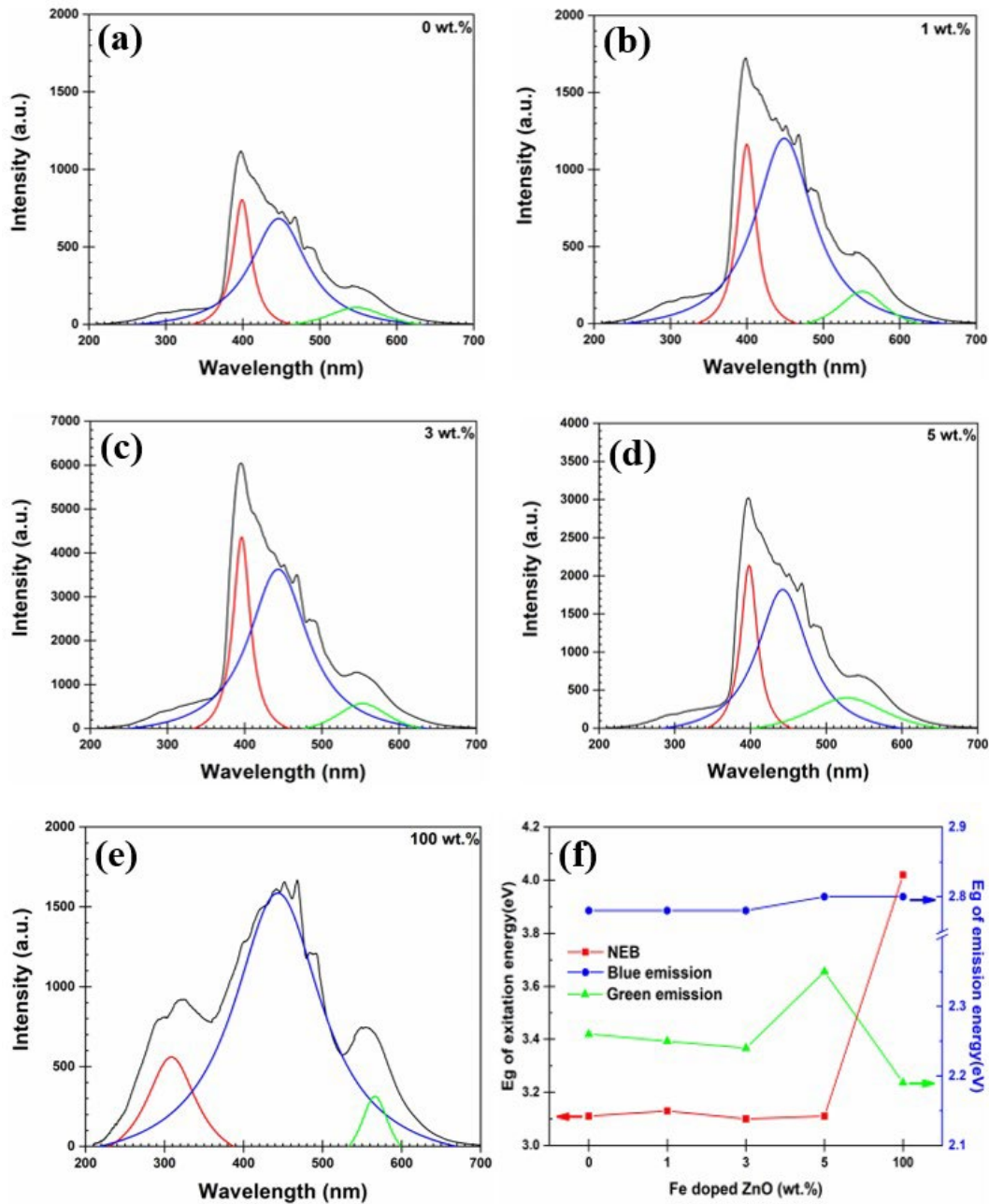


Figure 6. (a-e) Fluorescence spectrum with three peaks obtained from the Lorentzian fit of Fe-doped ZnO for 0, 1, 3, 5, and 100 wt.%, (f) The relationship between the energy band gap (E_g) for the near-band-edge (NBE), blue, and green emissions of Fe-doped ZnO samples.

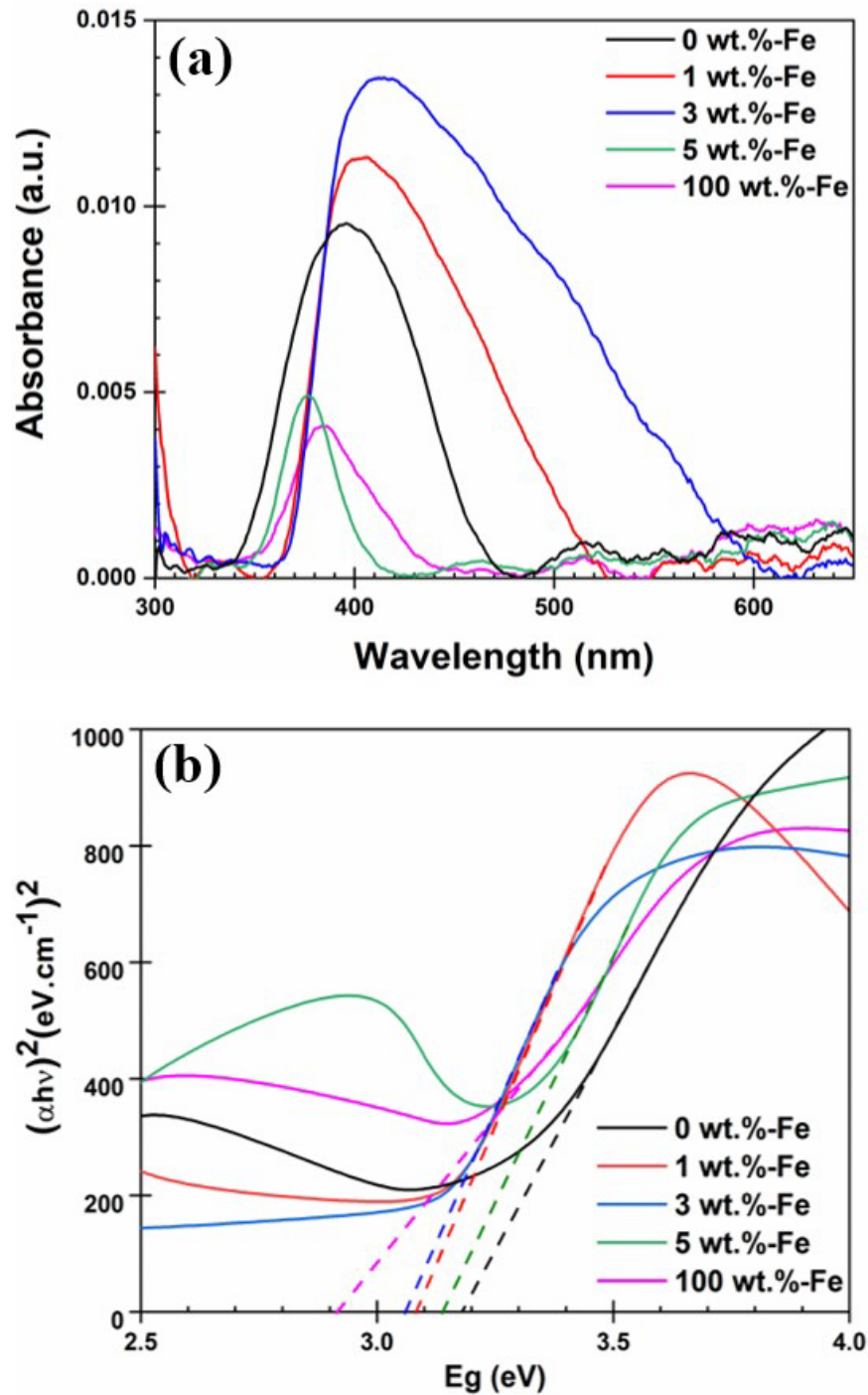


Figure 7. (a) Absorbance spectra from the UV-VIS spectrophotometer and (b) Plot of $(\alpha h\nu)^2$ versus the energy band gap (E_g) of Fe-doping ZnO NSs (0, 1, 3, 5 and 100 wt.%)

Figure 7(b) depicts the relationship between $(\alpha h\nu)^2$ and the energy band gap (E_g) of Fe-doped ZnO NSs at 0, 1, 3, 5 and 100 wt.% with an extrapolating line of E_g . The energy band gap from the absorbance spectra was calculated using Tauc's equation:

$$(\alpha h\nu)^n = A(h\nu - E_g) \quad (3)$$

where α is the absorbance coefficient, $h\nu$ is the photon energy (eV), A is the energy independent constant, E_g is the energy band gap (eV), $n = 2$ for an allowed indirect transition (Saadi et al., 2020; Gaur, 2021; Mohammadi, 2023). The E_g value of pure Fe_2O_3 (100 wt.%) was found to be 2.91 eV which was similar to the result of Al-Gaashani et al. (2014). The doping of Fe at 0, 1, 3, and 5 wt.% produced E_g values of 3.18, 3.09, 3.06, and 3.14 eV, respectively (Figure 6(b)) (Salem et al., 2016; Saadi et al., 2020; Roguai & Djelloul, 2021). Saadi et al. (2020) reported an E_g value of 3.19 eV for ZnO, and a range of 3.21, 3.18, and 3.02 eV for Fe-doped ZnO at 1, 5, and 10% which decreased with increasing Fe and showed a band gap of 3.02 eV as the minimum at 10%. Roguai & Djelloul (2021) prepared Fe-doped ZnO NPs of 0.00, 0.02, 0.05, and 0.10% by the co-precipitation method and observed an E_g value of 3.05-2.93 eV, which decreased with increasing Fe. However, in this report, it was found that the lowest E_g value for optical absorption was shown at doping of Fe at 3 wt.% in ZnO, as illustrated in Figure 7(b).

3.6 Electrical conductivity

Figure 8 presents the electrical conductivity and E_g value from optical absorption versus doping Fe of 0, 1, 3, 5 and 100 wt.%. It was observed that E_g decreased with increasing doping of Fe up to 3 wt.% and increased at doping Fe of 5 wt.% which was considered from the relation of E_g with Fe-doped ZnO. Many researchers found that increases in the doping agents such as copper, iron, cobalt and indium in ZnO caused decreases in the E_g value (Salem et al., 2016; Sajjad et al., 2018; Seid & Dejene, 2019; Saadi et al., 2020; Gaur et al., 2021; Roguai & Djelloul, 2021). It was observed the E_g value (Figure 7) was related the green emission (Figure 6(f)). The electrical resistance was measured by digital ohmmeter, as shown in Figure 1. The electrical resistance (R) value was an average of 5 tests (Montes et al., 2011; Wang et al., 2013). Electrical conductivity and electrical resistivity were calculated as follows;

$$\rho = RA / L \quad (4)$$

$$\sigma = 1 / \rho \quad (5)$$

where ρ is the electrical resistivity ($\Omega \cdot \text{cm}$), R is the electrical resistance (Ω), which was measured using the ohm meter, A is the surface area of the sample ($1 \times 1 \text{ cm}^2$), L is the thickness of the sample ($1 \mu\text{m}$), and σ is the electrical conductivity ($\Omega^{-1} \cdot \text{cm}^{-1}$). Therefore, in this research, the electrical conductivity of ZnO was found to be about $0.06 \times 10^{-3} \Omega^{-1} \cdot \text{cm}^{-1}$. The Fe-doped ZnO samples of 1, 3, and 5 wt.% exhibited the electrical conductivities of $0.13 \times 10^{-3} \Omega^{-1} \cdot \text{cm}^{-1}$, $0.21 \times 10^{-3} \Omega^{-1} \cdot \text{cm}^{-1}$ and $0.16 \times 10^{-3} \Omega^{-1} \cdot \text{cm}^{-1}$, respectively, as presented in Figure 8. Interestingly, the Fe-doped ZnO samples appeared to have higher electrical

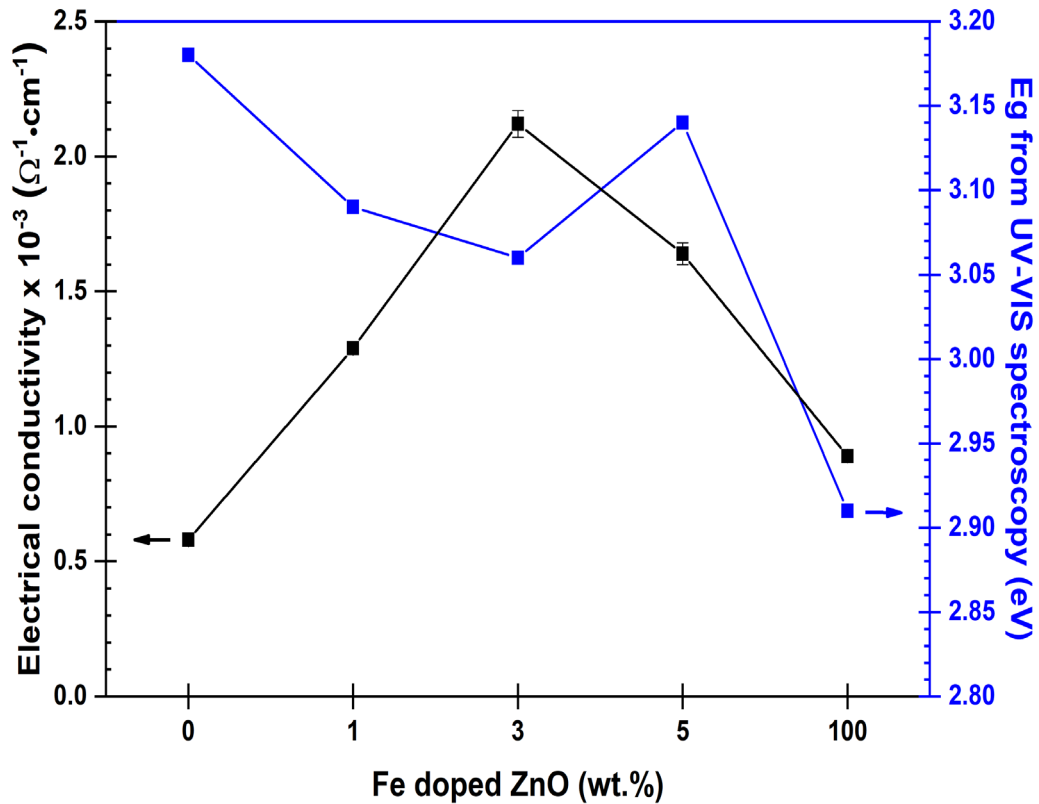


Figure 8. The relationship between electrical conductivity and all samples, varying the Fe doping levels from 0 to 100 wt.%, is depicted.

conductivity than that of the pure ZnO sample. Wang et al. (2013) found that the different morphologies of ZnO powder had different electrical resistances in the range of $(0.7621\text{--}21.0285) \times 10^8 \Omega$. Selvanayaki et al. (2022) investigated the electrical conductivity of pure ZnO and Fe-doped ZnO powder with doping of 3 to 5% and observed a decreasing trend of electrical conductivity of $0.081 \times 10^{-5} \Omega^{-1}\cdot\text{cm}^{-1}$, 0.063×10^{-5} and $0.025 \times 10^{-5} \Omega^{-1}\cdot\text{cm}^{-1}$, respectively. The electrical conductivity of Fe_2O_3 was shown to be about $0.09 \times 10^{-3} \Omega^{-1}\cdot\text{cm}^{-1}$, which appeared to be higher than that of Tahir et al. (2023). Tahir et al. (2023) found an electrical resistivity of $4.6 \times 10^9 \Omega\cdot\text{cm}$ ($2.17 \times 10^{-10} \Omega^{-1}\cdot\text{cm}^{-1}$) for hematite $\alpha\text{-Fe}_2\text{O}_3$ nanoparticles. It was noted that the electrical conductivity observed in this research was higher than the values reported by Wang et al. (2013) and Selvanayaki et al. (2022). The sample with 3 wt.% Fe doping exhibited the highest electrical conductivity and the lowest energy band gap. This enhancement is attributed to the minimum oxygen content and maximum Fe content observed at 3 wt.% doping in the EDS analysis. Additionally, a synergistic effect between oxygen vacancies and Fe ion incorporation, with oxygen vacancies, acts as electron donors and Fe ions altering the band structure. Therefore, Fe doping at 3 wt.% in ZnO appears to be optimal for improving the optical energy band gap (E_g) value and the electrical conductivity.

4. Conclusions

The properties of ZnO nanomaterials were enhanced through Fe doping via the co-precipitation method using a ZnCl₂ precursor doped with varying levels of FeSO₄ (0, 1, 3, 5, and 100 wt.%). The resulting precipitate was calcinated, and the nanomaterials underwent characterization for surface morphology, structure, and optical and electrical properties. SEM morphological analysis revealed the formation of nanoparticles in the non-doped ZnO and Fe₂O₃, while nanorods were observed in the Fe-doped ZnO samples. A transition in morphology from nanoparticle to nanorod was evident with increasing Fe doping. Elemental composition analysis by EDS confirmed the presence of the elements Zn, O, and Fe in the doped samples. Fe content was clearly detected starting at 3 wt.% doping. The fluorescence spectra were simulated with the three peaks as the near-band edge, and blue and green emissions. Fluorescence spectroscopy indicated changes in emission bands, and UV-VIS spectrophotometry showed absorption peaks at varying wavelengths for different doping levels. Moreover, the luminescence intensity of the Fe-doped samples exceeded that of the non-doped samples. The energy band gap (E_g) from both spectroscopies suggested optimal Fe doping at 3 wt.%. Electrical conductivity measurements demonstrated that Fe-doped ZnO exhibited higher conductivity compared to non-doped ZnO, with the highest conductivity observed at 3 wt.% Fe doping. In conclusion, this research highlights the potential of Fe doping through the co-precipitation method to enhance the electrical properties of ZnO nanomaterials. The tailored enhancement of ZnO nanomaterials through controlled Fe doping provides insights into potential applications in optoelectronics and related fields.

5. Acknowledgements

The authors would like to thank Graduate School, Nakhon Ratchasima Rajabhat University, Thailand, for their research funding, and Dr. Panadda Phansamdaeng, Mr. Samart Tuaykratok and Mr. Keardtpong Jadnok for their help with the XRD and fluorescence spectroscopy.

6. Conflicts of Interest

The authors declare that they have no conflicts of interest.

ORCID

Buppachat Toboosung  <https://orcid.org/0000-0003-2258-3860>

References

- Ahmad, F., & Maqsood, A. (2022). Influence of nickel dopant on impedance, dielectric, and optical properties of ZnO nanoparticles at low temperatures. *Journal of Materials Science: Materials in Electronics*, 33, 12674-12700.
- Alavi, M., Karimi, N., & Valadbeigi, T. (2019). Antibacterial, antibiofilm, antiquorum sensing, antimotility, and antioxidant activities of green fabricated Ag, Cu, TiO₂, ZnO, and Fe₃O₄ NPs via Protopermaliopsis muralis Lichen Aqueous extract against multi-drug-resistant bacteria. *ACS Biomaterials Science & Engineering*, 5(9), 4228-4243. <https://doi.org/10.1021/acsbiomaterials.9b00274>

- Al-Gaashani, R., Radiman, S., Tabet, N., & Daud, A. R. (2014). Rapid synthesis and optical properties of hematite (α -Fe₂O₃) nanostructures using a simple thermal decomposition method. *Journal of Alloys and Compounds*, 550, 395-401. <https://doi.org/10.1016/j.jallcom.2012.10.150>
- Alsmadi, A. K. M., Salameh, B., & Shatnawi, M. (2020). Influence of oxygen defects and their evolution on the ferromagnetic ordering and band gap of Mn-doped ZnO films. *The Journal of Physical Chemistry C*, 124(29), 16116-16126. <https://doi.org/10.1021/acs.jpcc.0c04049>
- Asok, A., Gandhia, M. N., & Kulkarni, A. R. (2012). Enhanced visible photoluminescence in ZnO quantum dots by promotion of oxygen vacancy formation. *Nanoscale*, 4(16), 4943-4946. <https://doi.org/10.1039/C2NR31044A>
- Baek, S., Song, J., & Lim, S. (2007). Improvement of the optical properties of ZnO nanorods by Fe doping. *Physica B: Condensed Matter*, 399(2), 101-104. <https://doi.org/10.1016/j.physb.2007.05.030>
- Cheng, W., & Ma, X. (2009). Structural, optical and magnetic properties of Fe-doped ZnO. *Journal of Physics: Conference Series*, 152, Article 012039. <https://doi.org/10.1088/1742-6596/152/1/012039>
- Divya, J., Pramothkumar, A., Gnanamuthu, S. J., Victoria, D. C. B., & Prabakar, P. C. J. (2020). Structural, optical, electrical and magnetic properties of Cu and Ni doped SnO₂ nanoparticles prepared via Co-precipitation approach. *Physica B: Condensed Matter*, 588, Article 412169. <https://doi.org/10.1016/j.physb.2020.412169>
- Gandhi, V., Ganesan, R., Syedahamed, H. H. A., & Thaiyan, M. (2014). Effect of cobalt doping on structural, optical, and magnetic properties of ZnO nanoparticles synthesized by coprecipitation method. *The Journal of Physical Chemistry C*, 118(18), 9715-9725. <https://doi.org/10.1021/jp411848t>
- Gaur, L. K., Gairola, P., Gairola, S. P., Mathpal, M. C., Kumar, P., Kumar, S., Kushavah, D., Agrahari, V., Aragon, F. F. H., Soler, M. A. G., & Swart, H. C. (2021). Cobalt doping induced shape transformation and its effect on luminescence in zinc oxide rod-like nanostructures. *Journal of Alloys and Compounds*, 868, Article 159189. <https://doi.org/10.1016/j.jallcom.2021.159189>
- Khan, K., Shah, M. Z. U., Aziz, U., Hayat, K., Sajjad, M., Ahmad, I., Ahmad, S. A., Shah, S. K., & Shah, A. (2022a). Development of 1.6 V hybrid supercapacitor based on ZnO nanorods/MnO₂ nanowires for next-generation electrochemical energy storage. *Journal of Electroanalytical Chemistry*, 922, Article 116753. <https://doi.org/10.1016/j.jelechem.2022.116753>
- Khan, M. A., Nayan, N., Ahmad, M. K., Fhong, S. C., Ali, M. S. M., Mustafa, M. K., & Tahir, M. (2022b). Interface study of hybrid CuO nanoparticles embedded ZnO nanowires heterojunction synthesized by controlled vapor deposition approach for optoelectronic devices. *Optical Materials*, 117, Article 111132. <https://doi.org/10.1016/j.optmat.2021.111132>
- Kumar, G. M., Ilanchezhian, P., Kawakita, J., Park, J., & Jayavel, R. (2013). Suppression of defect level emissions in low temperature fabricated one-dimensional Mn doped ZnO nanorods. *Journal of Materials Science: Materials in Electronics*, 24, 2989-2994. <https://doi.org/10.1007/s10854-013-1201-7>
- Mahajan, P., Singh, A., & Arya, S. (2022). Improved performance of solution processed organic solar cells with an additive layer of sol-gel synthesized ZnO/CuO core/shell nanoparticles. *Journal of Alloys and Compounds*, 814, Article 152292. <https://doi.org/10.1016/j.jallcom.2019.152292>
- Mayandi, J., Madathil, R. K., Abinaya, C., Bethke, K., Venkatachalapathy, V., Rademann, K., Norby, T., & Finstad, T. G. (2021). Al-doped ZnO prepared by co-precipitation

- method and its thermoelectric characteristics. *Materials Letters*, 288, Article 129352. <https://doi.org/10.1016/j.matlet.2021.129352>
- Meybodi, S. M., Hosseini, S. A., Rezaee, M., Sadmezhad, S. K., & Mohammadyani, D. (2012). Synthesis of wide band gap nanocrystalline NiO powder via a sonochemical method. *Ultrasonics Sonochemistry*, 19(4), 841-845. <https://doi.org/10.1016/j.ultsonch.2011.11.017>
- Mohammadi, M., Sabbaghi, S., Binazadeh, M., Ghaedi, S., & Rajabi, H. (2023). Type-1 α -Fe₂O₃/TiO₂ photocatalytic degradation of tetracycline from wastewater using CCD-Based RSM optimization. *Chemosphere*, 336, Article 139311. <https://doi.org/10.1016/j.chemosphere.2023.139311>
- Montes, J. M., Cuevas, F. G., & Cintas, J. (2011). Electrical conductivity of metal powder aggregates and sintered compacts. *Granular Matter*, 13, 439-446. <https://doi.org/10.1007/s10035-010-0246-z>
- Montes, J. M., Cuevas, F. G., Cintas, J., & Gallardo, J. M. (2016). Electrical conductivity of metal powder aggregates and sintered compacts. *Journal of Materials Science*, 51, 822-835. <https://doi.org/10.1007/s10853-015-9405-2>
- Nadeem, M. S., Munawar, T., Mukhtar, F., Rahman, M. N., Riaz, M., & Iqbal, F. (2021). Enhancement in the photocatalytic and antimicrobial properties of ZnO nanoparticles by structural variations and energy bandgap tuning through Fe and Co co-doping. *Ceramics International*, 47(8), 11109-11121. <https://doi.org/10.1016/j.ceramint.2020.12.234>
- Nakate, U. T., Patil, P., Na, S.-N., Yu, Y. T., Suh, E.-K., & Hahn, Y.-B. (2021). Fabrication and enhanced carbon monoxide gas sensing performance of p-CuO/n-TiO₂ heterojunction device. *Colloids and Surfaces A: Physicochemical and Engineering Aspects*, 612, Article 125962. <https://doi.org/10.1016/j.colsurfa.2020.125962>
- Niranjan, K., Dutta, S., Varghese, S., Ray, A. K., & Barshilia, H. C. (2017). Role of defects in one-step synthesis of Cu-doped ZnO nano-coatings by electrodeposition method with enhanced magnetic and electrical properties. *Applied Physics A*, 123, Article 250. <https://doi.org/10.1007/s00339-017-0890-9>
- Pramothkumar, A., Senthilkumar, N., Jenila, R. M., Durairaj, M., Girisun, S. T. C., & Potheher, I. V. (2021). A study on the electrical, magnetic and optical limiting behaviour of Pure and Cd-Fe co-doped CuO NPs. *Journal of Alloys and Compounds*, 878, Article 160332. <https://doi.org/10.1016/j.jallcom.2021.160332>
- Roguai, S., & Djelloul, A. (2021). Structural, microstructural and photocatalytic degradation of methylene blue of zinc oxide and Fe-doped ZnO nanoparticles prepared by simple coprecipitation method. *Solid State Communications*, 334-335, Article 114362. <https://doi.org/10.1016/j.ssc.2021.114362>
- Saadi, H., Rhouma, F. I. H., Benzarti, Z., Bougrioua, Z., Guermazi, S., & Khirouni, K. (2020). Electrical conductivity improvement of Fe doped ZnO nanopowders. *Materials Research Bulletin*, 129. <https://doi.org/10.1016/j.materresbull.2020.110884>
- Sajjad, M., Ullah, I., Khan, M. I., Khan, J., Khan, M. Y., & Qureshi, M. T. (2018). Structural and optical properties of pure and copper doped zinc oxide nanoparticles. *Results in Physics*, 9, 1301-1309. <https://doi.org/10.1016/j.rinp.2018.04.010>
- Salem, M., Akir, S., Ghrib, T., Daoudi, K., & Gaidi, M. (2016). Fe-doping effect on the photoelectrochemical properties enhancement of ZnO films. *Journal of Alloys and Compounds*, 685, 107-113. <https://doi.org/10.1016/j.jallcom.2016.05.254>
- Samanta, A., Goswami, M. N., & Mahapatra, P. K. (2018). Magnetic and electric properties of Ni-doped ZnO nanoparticles exhibit diluted magnetic semiconductor in nature. *Journal of Alloys and Compounds*, 730, 399-407. <https://doi.org/10.1016/j.jallcom.2017.09.334>
- Sangchay, W., & Ubolchollakhat, K. (2016). Photocatalytic and antibacterial activities of ZnO powders prepared via a sol-gel method. *KKU Engineering Journal*, 43(1), 21-25.

- Seid, E. T., & Dejene, F. B. (2019). Controlled synthesis of In-doped ZnO: the effect of indium doping concentration. *Journal of Materials Science: Materials in Electronics*, 30, 11833-11842. <https://doi.org/10.1007/s10854-019-01557-w>
- Selvanayaki, R., Rameshbabu, M., Muthupandi, S., Razia, M., Sasi, F. S., Ravichandran, K., & Prabha, K. (2022). Structural, optical and electrical conductivity studies of pure and Fe doped ZincOxide (ZnO) nanoparticles. *Materials Today: Proceedings*, 49, 2628-2631. <https://doi.org/10.1016/j.matpr.2021.08.045>
- Sharma, D., & Jha, R. (2017). Analysis of structural, optical and magnetic properties of Fe/Co co-doped ZnO nanocrystals. *Ceramics International*, 43(11), 8488-8496. <https://doi.org/10.1016/j.ceramint.2017.03.201>
- Singh, J., & Singh, R. C. (2021). Tuning of structural, optical, dielectric and transport properties of Fe-doped ZnO:V system. *Materials Science in Semiconductor Processing*, 121. <https://doi.org/10.1016/j.mssp.2020.105305>
- Sugumaran, S., Ahmad, M. N. B., Jamlos, M. F., Bellan, C. S., Pattiyappan, S., Rajamani, R., & Sivaraman, P. K. (2021). Transparent with wide band gap In-ZnO nano thin film: Preparation and characterizations. *Optical Materials*, 49, 348-356. <https://doi.org/10.1016/j.optmat.2015.10.003>
- Tahir, M., Fakhar-e-Alam, M., Atif, M., Mustafa, G., & Ali, Z. (2023). Investigation of optical, electrical and magnetic properties of hematite α -Fe₂O₃ nanoparticles via sol-gel and co-precipitation method. *Journal of King Saud University - Science*, 35(5), Article 102695. <https://doi.org/10.1016/j.jksus.2023.102695>
- Thandavan, T. M. K., Wong, C. S., Gani, S. M. A., & Nor, R. M. (2014). Photoluminescence properties of un-doped and Mn-doped ZnO nanostructures. *Materials Express*, 4(6), 475-482. <https://doi.org/10.1166/mex.2014.1193>
- Toboosung, B., & Singjai, P. (2011). Formation of CuO nanorods and their bundles by an electrochemical dissolution and deposition process. *Journal of Alloys and Compounds*, 509(10), 4132-4137. <https://doi.org/10.1016/j.jallcom.2010.12.180>
- Toboosung, B. (2017). Structure, magnetic property and energy band gap of Fe-doped NiO nanoparticles prepared by co-precipitation method. *Key Engineering Materials*, 751, 379-383. <https://doi.org/10.4028/www.scientific.net/KEM.751.379>
- Wang, H., Li, C., Zhao, H., Li, R., & Liu, J. (2013). Synthesis, characterization, and electrical conductivity of ZnO with different morphologies. *Powder Technology*, 239, 266-271. <https://doi.org/10.1016/j.powtec.2012.12.045>
- Zeng, H., Duan, G., Li, Y., Yang, S., Xu, X., & Cai, W. (2010). Blue luminescence of ZnO nanoparticles based on non-equilibrium processes: Defect origins and emission controls. *Advanced Functional Materials*, 20(4), 561-572. <https://doi.org/10.1002/adfm.200901884>
- Zhu, L., Zheng, Y., Hao, T., Shi, X., Chen, Y., & Ou-Yang, J. (2009). Synthesis of hierarchical ZnO nanobelts via Zn(OH)F intermediate using ionic liquid-assistant microwave irradiation method. *Materials Letters*, 63(28), 2405-2408. <https://doi.org/10.1016/j.matlet.2009.07.062>